# Cyclic Triaxial Testing on Undisturbed Samples of Rhyolitic Material from the Waikato Region.

Report Number: OG17-01

Prepared for: Stephen Christensen, Anderson Lloyd

Prepared by: Mark Stringer, University of Canterbury

Date: 5th April 2018

Version: 1.0



UC
UNIVERSITY OF CANTERBURY
Te Whare Wānanga o Waitaha
CHRISTCHURCH NEW ZEALAND

# Introduction

This report describes the suite of cyclic triaxial testing which has been undertaken at the University of Canterbury on undisturbed specimens of rhyolitic deposits from the locations of AP12a, AP13a and AP14a close to Waihi. The main body of the report contains descriptions of laboratory procedures and a summary of the testing and results from the triaxial testing. Detailed plots of test data for each specimen is provided in the appendices.

Testing on the specimens was conducted in two series: the first (on specimens from AP13a at approx. 10 -12m depth) involved testing at 1.05 times the estimated in-situ effective stresses (assuming a saturated unit weight of 16kN/$m^3$ and a water table depth of 0.5m as advised by Engineering Geology Ltd). The second test series involved testing specimens at 400kPa to investigate the behaviour of the material under elevated stress levels.

# Key observations from site visit and laboratory testing

In the process of conducting a visit to the borehole locations and subsequent laboratory testing, a number of important features have been observed relating to the soils being tested.

## Observations from site visit

- At the location of the boreholes, it was apparent that the soil profile is highly variable. Though the material appears to be consistent in terms of composition, it appeared that there are both sections of the profile which are relatively stiff and strong (likely cemented) as well as material which is extremely soft and claylike, and with high water content. The vertical transition from the stiff material to the soft material was in places extremely sharp.
- It will be important to assess the lateral extents of the different materials, and whether the softer material forms a continuous lens/layer.

## Observations from testing

- The isotropic consolidation curves indicate a yield point for these soils in the region of 200kPa.
- The void ratios of the material at the time of testing are extremely high, and are more representative in broad terms of a clayey material than a sand.
- Despite the soil material being relatively fine grained, the primary consolidation of these soils was completed extremely quickly. However, it was notable that these soils undergo significant secondary consolidation under high effective stress, with minor volumetric and axial strains continuing to accumulate after extended periods. The ultimate volumetric and axial strains associated with this secondary consolidation were often large both in absolute terms, and relative to the primary consolidation. The consolidation behaviour suggests to the author that the material should be considered to have a double porosity characteristic such that the material might be thought of being composed of agglomerations of finer material. This would explain the very high hydraulic conductivity and the large secondary consolidation. **The overall behaviour indicates that significant consolidation settlements should be expected to develop over significant time periods if the full soil deposit is loaded beyond the yield stress**.
- During cyclic loading, excess pore water pressures developed, but at the point of "failure," the excess pore water pressure ratios ($r_u$) tended to be in the range of 0.8-0.9. Typically, excess pore water pressures in sand-like materials undergoing liquefaction would be expected to

have $r_u$ values close to 1 (i.e. zero effective stress) at instants when deviator stress is zero. The pore water pressure response is more typical of a clay-like material.

- The number of cycles to failure is clearly linked to the magnitude of shear stresses being applied. However, the failures observed during the testing were mainly brittle in nature, with a split developing on the extensional side of loading at strain levels typically around 2-3%. **The brittle nature of the failures observed during the testing should be specifically considered in the final assessment of stability since it implies that if loading (seismic of otherwise) causes a similar failure to develop in the field, then there is the potential for large movements to occur extremely rapidly**. A key factor governing whether or not this occurs is the spatial extent of the material.
- **The failure of these specimens should not be considered to be liquefaction or representative of sandy material.**

## Identifying Samples

Throughout this report, sample refers to the complete soil column retrieved by the sampler, while specimen refers to the section of a soil sample which has been tested in one of the triaxial devices. Additionally, specimens are referred to using a 4 part naming convention:

ww-xx-yy-zz

- ww: location reference where the sampling took place
- xx: type of sampler and borehole number at the specific location
- yy: sample number within borehole xx
- zz: specimen ID within sample yy

The codes used for the different specimens are summarized in Table 1

*Table 1: Specimen identification*

| Borehole ID | Sample Depth (m) | Specimen ID | Specimen Mid Depth (m) |
|---|---|---|---|
| AP12a | 13.70-14.15 | AP12a-DM1-4-A | 13.81 |
| | | AP12a-DM1-4-B | 13.93 |
| | | AP12a-DM1-4-C | 14.05 |
| | 19.70-20.15 | AP12a-DM1-6-A | 19.81 |
| | | AP12a-DM1-6-B | 19.93 |
| | | AP12a-DM1-6-C | 20.05 |
| AP13a | 10.10-10.55 | AP13a-DM1-1-A | 10.25 |
| | | AP13a-DM1-1-B | 10.4 |
| | 12.10-12.55 | AP13a-DM1-2-A | 12.26 |
| | | AP13a-DM1-2-B | 12.45 |
| | 16.00-16.45 | AP13a-DM1-4-A | 16.17 |
| | | AP13a-DM1-4-B | 16.27 |
| AP14a | 15.20-15.65 | AP14a-DM1-6-A | 15.29 |

## Description of Triaxial Device

A DTC-367 triaxial testing system, manufactured by Seiken Ltd, was used for the testing described in this report. Key elements of this system are shown in Figure 1.

During testing the triaxial cell is filled with water above the level of the top platen, but leaving an air gap at the top of the cell. The cell is pneumatically pressurised using the central compressed air supply, and cell pressure is measured at the base of the cell. Back-pressures can be applied to the specimen through either of the top or bottom drainage lines, with pressures being measured on the bottom drainage line, at the same elevation as the cell pressure transducer.

Axial displacements are measured using a linear variable displacement transducer, which measures the vertical displacement of the loading ram, external to the cell. The drainage from the specimen is monitored using a volume meter, which can accept drainage from both the top and bottom drainage lines.

Axial loads are measured inside the triaxial cell, using a pressure compensated 2kN load cell. Placement of the axial load cell within the triaxial cell provides a direct measurement of the loading on the specimen. The axial loading during cyclic loading is servo-controlled with closed-loop feedback. During a triaxial compression test, the position of the loading ram is locked in place, and the triaxial cell jacked vertically under displacement control.

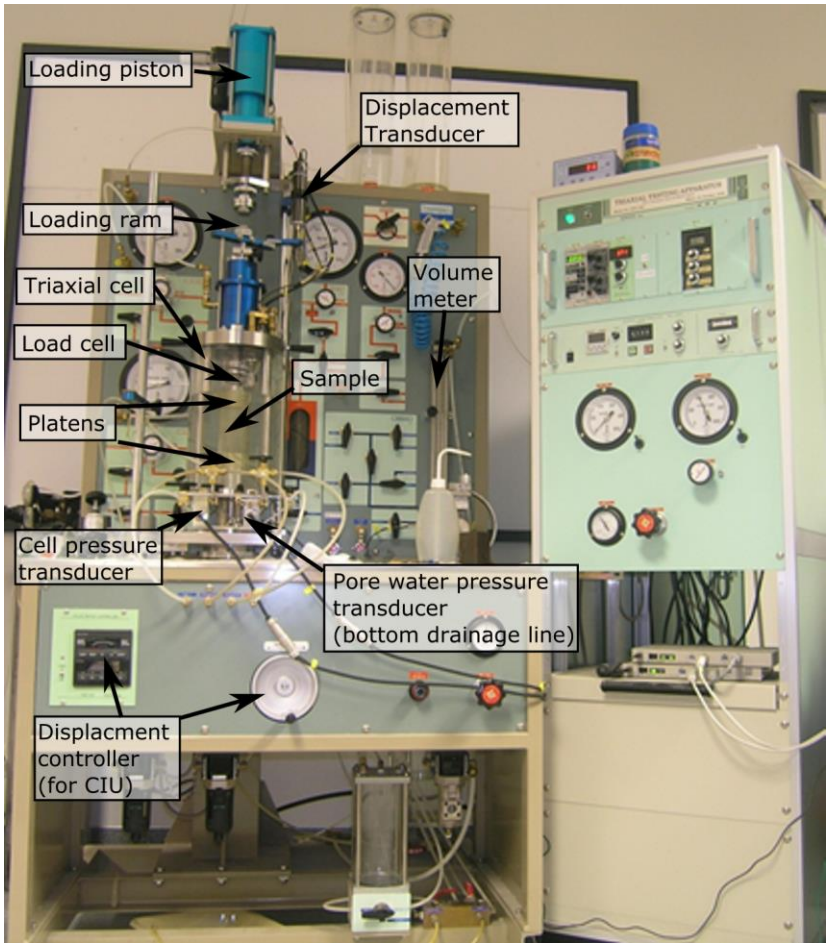


*Figure 1: Main components of triaxial device*

## Field Visit to Prepare Samples for Transportation

A visual inspection of the samples recovered from the site was undertaken prior to their transportation to the laboratories in Christchurch and Auckland. It had originally been anticipated that the samples should be frozen prior to transportation to preserve their density, structure and fabric. However, it has been shown in the literature that even relatively modest amounts of fine material can prevent the free draining of pore water from the material, and that in these cases, the process of freezing can result in significant damage to the soil sample (Singh et al. 1982).

On inspection of the samples in the field, it was apparent that the material was not suitable for freezing on account of the fine material (cemented or otherwise). It was also apparent that immediately after sampling, some limited drainage was occurring, which suggested that the air entry value of the specimens was too low to preserve the mean in-situ stress level.

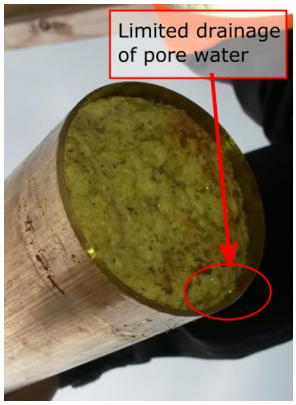


*Figure 2: Partial drainage on sample in the field*

On the basis of the high fines content and the limited on site drainage, it was decided to allow the samples to naturally drain, using a damp cloth to help draw free water from the sample. The samples were then wrapped in foam padding to try to isolate the samples from harmful vibrations during transportation.

Two samples were hand carried back to Christchurch (by the author), and one of the tubes was immediately inspected on arrival in the laboratory. It was observed that there were

- no obvious signs of disturbance
- no obvious sign of additional water (i.e. as a result of densification)
- no obvious change in the height of the sample (i.e. the length of the soil column)

Based on these observations, the same technique was used for the transportation of the remaining samples.

While on site, the author observed the material which was obtained by rotary coring for logging purposes. It was apparent at this stage that the material was very variable, with some portions of the core appearing to be extremely stiff, with apparent cementation. On the other hand, some portions of the borehole were noticeable softer, resembling a very soft clay-like material. The transition between these two different types of material could occur over a very short spatial distance. The detailed logging of these different materials was carried out by the site engineer, and due consideration should be given to the extent of the material variability, which may not have been fully captured in the samples which have been tested in the laboratory.

## Laboratory Procedures.

Individual soil specimens for triaxial testing were obtained from *Dames & Moore (DM) hydraulic fixed piston with thin constant diameter brass tubes* received from OceanaGold. DM sampling has been used in a number of research applications (both in New Zealand and globally) to obtain high quality soil samples, and the visual appearance of the samples in the laboratory appears to indicate that the sampling was successful in terms of obtaining quality soil samples for testing.

It is anticipated that the material at the extreme ends of the tube are disturbed as a result of drilling the borehole (disturbance at the top of the sample) and from pulling the specimen out of the hole after sampling (disturbance at the bottom of the sample). The material from either end of the sample tubes are generally excluded from testing.

Individual specimens were extruded from the push tubes. To reduce the total load required to extrude the specimen (which may cause disturbance), the tubes were pre-cut using a pipe cutter slightly above and below the intended location of the specimen. Stiffening rings were clamped to the tube (Figure 3 a) above and below the location of the pipe cutter to prevent ovalling of the thin-walled sample tube. A wire saw was used to cut through the sample at the location of the cuts.

Prior to extrusion, the burrs created by the pipe cutter at the top cut were removed using a deburring tool. To facilitate this process, a 1cm ring of soil about 0.5cm deep was removed from the top of the specimen (Figure 3 b). Once the tube had been deburred, the specimen was extruded using a hydraulic piston, from bottom to top.

A small number of specimens were tested without reducing the specimen diameter. For these specimens, the first 1cm of soil was extruded and then removed with a wire saw prior to being encased in a latex membrane.

The majority of specimens were tested with a nominal diameter of 50mm. These specimens were trimmed in a soil lathe using a sharp knife (Figure 3 c). After reducing the diameter of the specimen to 50mm, the specimen was placed in a mitre box (Figure 3 d), and soil carefully cut from both ends so that the total length was approximately 100mm. Trimmed specimens were encased in a latex membrane prior to mounting in the device.

Shear wave velocity was measured on a number of the specimens using bender elements mounted in the platens of the triaxial device. To facilitate the entry of the bender elements, small slots were cut into the ends of the specimens using a razor blade (Figure 3 e).

Specimens were mounted in the triaxial device, and approximately 20kPa vacuum (larger vacuums were applied for some tests where the test pressure was specified as 400kPa) was applied to allow the initial diameter and height of the specimen to be measured. The diameter was measured using a pi-tape, while height is inferred from the difference in the displacement transducer reading when a spacer of known height is placed between the platens.

It should be noted that the material in these specimens was in some cases quite variable, with hard grained coarse sand, friable gravel-sized material and soft residual material all encountered. This variability created some difficulties in the trimming, where the hard sand or friable material would tend to “flick out” of the specimen as it was trimmed, creating surface voids. Where these created large voids, an attempt was made to infill the gap using the material which had previously been trimmed from the specimen.

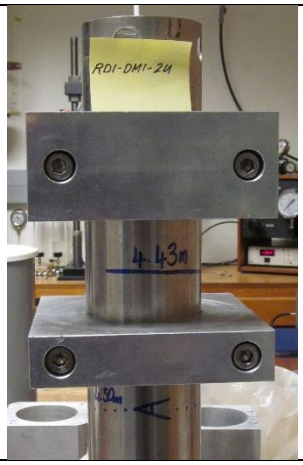


(a) Stiffening rings to prevent ovalling

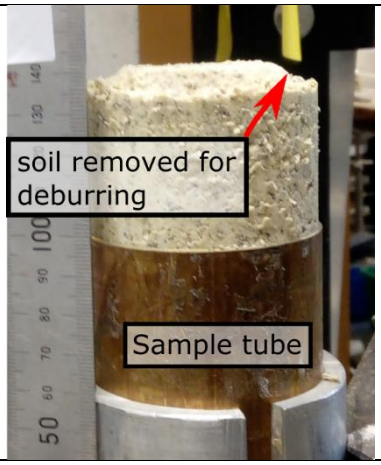


(b) Removing soil to enable deburring

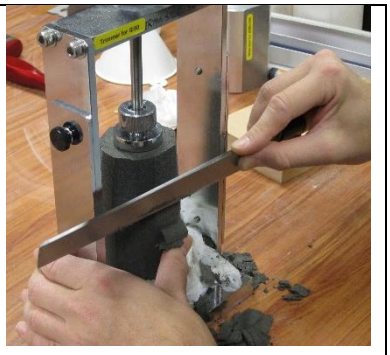

(c) Reducing specimen diameter in a lathe

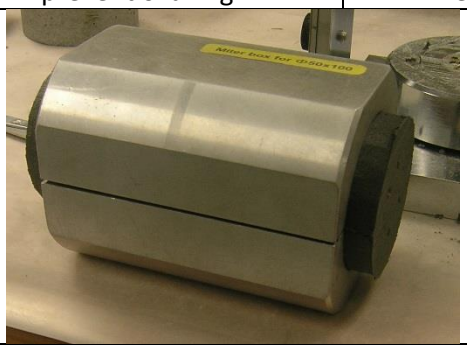

(d) Mitre box for facing specimen ends

(e) Slot for inserting the bender element

*Figure 3: Laboratory procedures (note photos a, c and d were taken from testing on a different research project)*

Soil specimens were saturated following a two step-process. $CO_2$ was percolated through the soil specimen at a slow rate, before percolating at least two sample volumes of de-aired water through the specimen. For soil specimens being tested at close to their in-situ stress levels, it was possible to complete saturation by the application of "back-pressure" while maintaining the current level of effective stress. This however required back pressures in excess of 400kPa. Saturation was deemed complete once a B-value in excess of 0.97 was recorded (Skempton, 1954).

$$B = \frac{\Delta u}{\Delta p} \quad (1)$$

To allow testing of specimens at an effective confining pressure of 400kPa, a large vacuum (typically 85-90kPa) was applied to the specimens after percolating $C0_2$ and deaired water. Vacuum was also applied to the triaxial cell to maintain the effective stresses during the test. This additional process enabled saturation to be completed with back pressures which were typically less than 200kPa.

Fully saturated specimens were isotropically consolidated to the target effective stress level for the test. Consolidation was carried out in a number of steps, with drainage permitted through the top of the specimen only, while pore water pressures are measured at the base of the specimen. This means that the largest excess pore water pressures present in the specimen can be accurately monitored (i.e. using this setup, primary consolidation is known to be complete once the measured excess pore water pressures return to zero). The rapid dissipation of excess pore water pressures meant that for many of the early tests, it was possible to increase the cell pressures slowly so that the excess pore water pressures were close to zero throughout. In later tests, it was decided to revert back to a stepped consolidation process, where the cell pressure was incrementally increased, with drainage permitted after the increment of cell pressure, and through the top drainage line only. **It should be noted that**

**while excess pore water pressures dissipated rapidly, a large amount of secondary consolidation accumulated at confining pressures larger than the in-situ stresses. In the tests carried out with a mean confining pressure of 400kPa, the samples were typically left overnight (i.e. 8-9 hours) to allow the volume of the specimen to stabilize.**

The B-value of the specimen was measured immediately prior to the commencement of cyclic loading. These values would typically reduce during the consolidation phase. The post-consolidation B-values are reported in the summary of test results.

Cyclic loading was applied at a nominal frequency of 0.1Hz, with a range of cyclic stress ratios (CSR, defined in Equation 2) being applied in the tests. The cyclic loads were typically halted once the peak to peak axial strain reached 5% (a common definition of "liquefaction" in the laboratory), or once several hundred cycles of load had been applied.

$$CSR = \frac{q}{2p_0'} \quad (2)$$

Following the cyclic loading, the specimen was either reconsolidated (top drainage only) back to its original stress level to obtain the post-cyclic volumetric strain, or subjected to an undrained triaxial compression test. Triaxial compression tests were initially conducted at a rate of 1mm/min, however, this was reduced to 0.03mm/min for the final 2 tests, based on a discussion of the results with Engineering Geology.

In all cases, the soil specimen was split in half following testing to observe the interior of the specimen. Half of the soil was oven dried to obtain the dry mass of soil in the specimen.

## Shear wave velocity testing

Shear wave velocity testing was carried out on specimens which had been trimmed to 50mm diameter using bender elements. When carrying out these tests, a sinusoid voltage pulse is sent to the ``source'' bender element (mounted in a platen as shown in Figure 4b), which deflects under the voltage applied. This generates a horizontally orientated shear wave to propagate vertically through the specimen. When the shear wave arrives at the ``receiver'' bender element, it causes a small deflection of the bender element, which in turn generates a small voltage, which is monitored using an oscilloscope. This system is shown schematically in Figure 4(a), along with a photo of one of the bender elements used in the Seiken triaxial device. By considering the height of the specimen and the time difference between sending the voltage pulse and the first arrival of the shear wave, it is possible to estimate the shear wave velocity (Equation 3, where $l_{tt}$ is the distance between the tips of the bender elements). It should be noted that the source wave is not directly measured, but is assumed to be the same shape and occur at the same time as the output from the signal generator. In practice, there is a delay between the output of the signal generator and the displacement of the source bender element. The "system delay" is measured by holding the tips of the source and receiver elements together and measuring the time lag between the source signal and the received signal. For the testing presented in this report, the time delay is 11.1µs. This time delay was subtracted from the receiver signal prior to picking the arrival time.

$$v_s = \frac{l_{tt}}{t_{arr}} \tag{3}$$

$$v_{s1} = v_s \left(\frac{p_a}{p'}\right)^{0.25} \tag{4}$$

The interpretation of the shear wave arrival time remains subject to some debate in the literature. Figure 5 shows results from a typical bender element test. Marked on the figure are typical points which have been used by researchers to define the arrival time of the shear wave. Points SA and SB, refer to points on the source wave, while points RA, RB, RC & RD refer to points on the received waveform. Interpretations of the arrival time based on first arrival of the shear wave include the difference between SA and RA, RB, RC. An estimate of shear wave velocity can also be made using the time difference between the zero crossings linking the major peaks (SB and RD).

In this report, the "first arrival" time of the shear wave has been determined manually, using the point where the receiver signal begins its major departure (i.e. point RB) in the positive direction (the direction expected based on the polarity of the bender elements). In some cases, the arrival time has been picked later than the point where the received signal begins to deviate in the positive direction due to apparent changes in the gradient of the received signal, which suggests this alternative interpretation. The source and receiver bender element signals from each test are shown in the Appendix, along with markers indicated the picked arrival times. A second estimate of the shear wave velocity has been made based on the "zero crossing" method (i.e. points SB and RD) for comparison against the first arrival.

The shear wave velocity measurements were typically made at a range of confining pressures during the consolidation of the soil specimen. Despite initial success with the bender elements on a sample consolidated to 400kPa, the devices stopped working at high pressures. The bender elements continued to function up to a mean effective pressure of 200kPa, hence shear wave velocities were gathered up to this stress level.

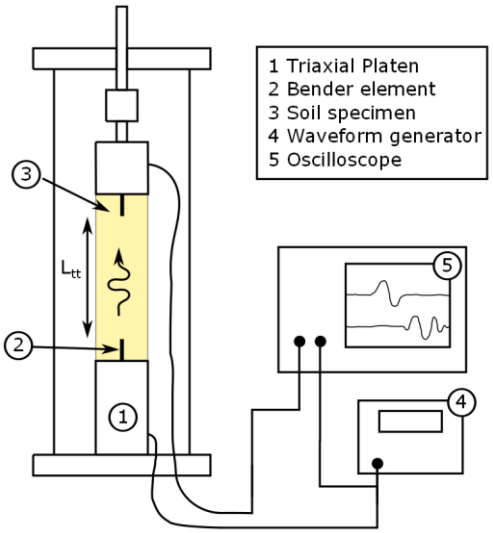


(a) Typical set-up for bender elements

(b) Bender element platen

*Figure 4: Bender element set-up*

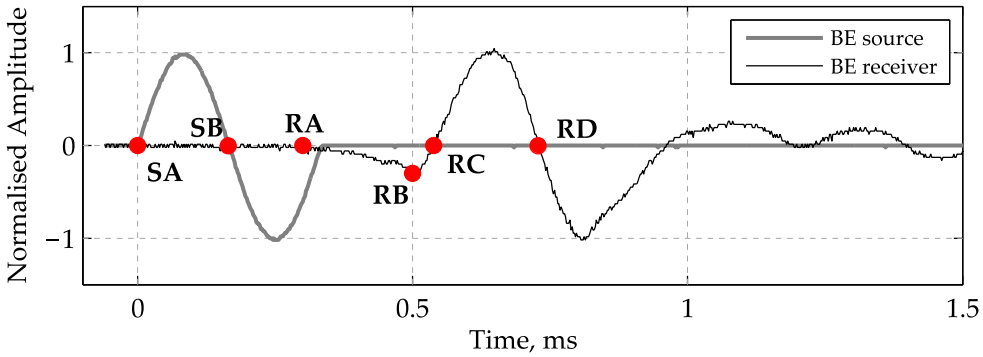


*Figure 5: Interpretation of arrival time*

## Data Summaries

The data and graphs shown in the following sections provide a summary of the testing carried out. The detailed test plots are presented in Appendix A, and contains notes related to known issues in the testing.

*Table 2: Summary of Test data*

| Tube | Mid Depth (m) | Test Date | B-Value | $p'_{field}$ (kPa) | $p'_{test}$ (kPa) | $\rho_{dry,test}$ (kg/m3) | f (Hz) | CSR | N5DA |
|---|---|---|---|---|---|---|---|---|---|
| AP12a-DM1-4 -A | 13.81 | 13/11/17 | 0.97 | 90.5 | 407.9 | 967 | 0.1 | 0.39 | 1* |
| AP12a-DM1-4 -B | 13.93 | 20/11/17 | | 91.3 | Sample developed leak during consolidation | | | | |
| AP12a-DM1-4- C | 14.05 | 04/12/17 | 0.95 | 92.0 | 407.7 | 962 | 0.1 | 0.33 | 4* |
| AP12a-DM1-6- A | 19.81 | 07/11/17 | 0.98 | 127.7 | 406.0 | 923 | 0.1 | 0.20 | 300†! |
| AP12a-DM1-6- B | 19.93 | 09/11/17 | 0.95 | 128.5 | 409.7 | 931 | 0.1 | 0.27 | 25 |
| AP12a-DM1-6- C | 20.05 | 10/11/17 | 0.95 | 129.2 | 408.5 | 910 | 0.1 | 0.31 | 10 |
| AP13a-DM1-1- A | 10.25 | 22/10/17 | 0.96 | 68.5 | 73.9 | 731 | 0.1 | 0.33 | 615.5† |
| AP13a-DM1-1 -B | 10.4 | 26/10/17 | | 69.4 | Sample developed leak during consolidation | | | | |
| AP13a-DM1-2 -A | 12.26 | 30/09/17 | 0.97 | 80.9 | 99.1 | 652 | 0.1 | 0.40 | 47.5 |
| AP13a-DM1-2 -B | 12.45 | 06/10/17 | 0.98 | 82.1 | 87.0 | 672 | 0.1 | 0.53 | 20* |
| AP13a-DM1-4 -A | 16.17 | 01/11/17 | 0.95 | 105.2 | 408.5 | 964 | 0.1 | 0.36 | 2 |
| AP13a-DM1-4 -B | 16.27 | 31/10/17 | | 105.8 | Sample developed leak during consolidation | | | | |
| AP14a-DM1-6 -A | 15.29 | 06/12/17 | 0.94 | 99.7 | 408.4 | 1047 | 0.1 | 0.34 | 2 |
| AP14a-DM1-6-B | 15.45 | 23/01/18 | 0.95 | 100.7 | 406.3 | 1125 | CIU test | | |

*: Number of cycles has been interpreted; see appendix for specific notes.
†: 5% double amplitude axial strain was not reached during the testing.
!:Pressure loss during consolidation.

## Consolidation

The void ratios at different mean effective stress levels during the consolidation phase of the experiment are shown in Figure 6. The void ratios have been calculated using the estimated dry mass of the specimen which was measured at the end of the experiment. To preserve some of the test material for potential future laboratory testing, the dry mass was estimated using the water content determined for half of the test specimen. Specific gravity has been assumed to be 2.65 for all specimens.

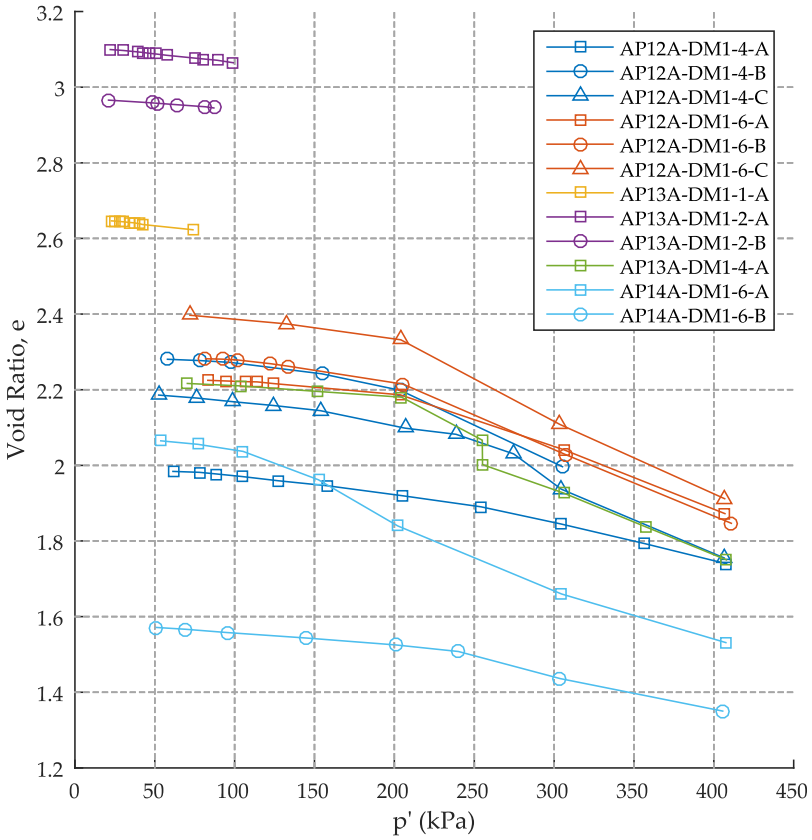


*Figure 6: Void ratios during consolidation of specimens*

Detailed data is shown for the consolidation of each experiment in the Appendices. As previously stated, the primary consolidation based on the dissipation of excess pore water pressure in these specimens was completed rapidly (typically within 30s of the start of consolidation). However, it was observed that beyond the yield stress, volumetric strains continued to accumulate for long time periods after the excess pore water pressures had returned to zero. The volumetric strains occurring during this secondary consolidation were often much larger than those associated with the primary consolidation. It should be expected that if these soils are loaded beyond their apparent yield stress, then large settlements should be expected over a significant time period.

Given the rapid dissipation of excess pore water pressures in the specimens and the large secondary consolidation, it is likely that attempts to accelerate the consolidation of these soils (i.e. constructing soil drains) would be unsuccessful.

## Shear Wave Velocity

Measurements of shear wave velocities from the consolidation phase of the experiments are summarised in Figure 7 ("first arrival" only), with numerical values shown in Table 3 (both "first arrival" and "zero crossing"). Details concerning the testing procedures are discussed in the "Laboratory Procedures" section of this report. The detailed test plots showing the raw data and selection of "first arrival" times are shown in the Appendix with the detailed test information.

Note that the shear wave velocities from "zero crossing" has typically been estimated for the lowest and highest mean effective confining pressures, and are included to give a sense of the variability according to the method of selection. In some cases, the received bender element signal was clipped prior to the zero crossing (i.e. AP12a-DM1-4-B), or the zero crossing was not clear (i.e. AP12a-DM1-6-A). In these cases, no data has been entered in Table 3. The final column of Table 3 indicates the difference between the two measurements at each frequency. It should be noted that in many cases, the zero crossing method showed a trend with frequency, which can occur when received signal pulse is not at the same frequency as the input.

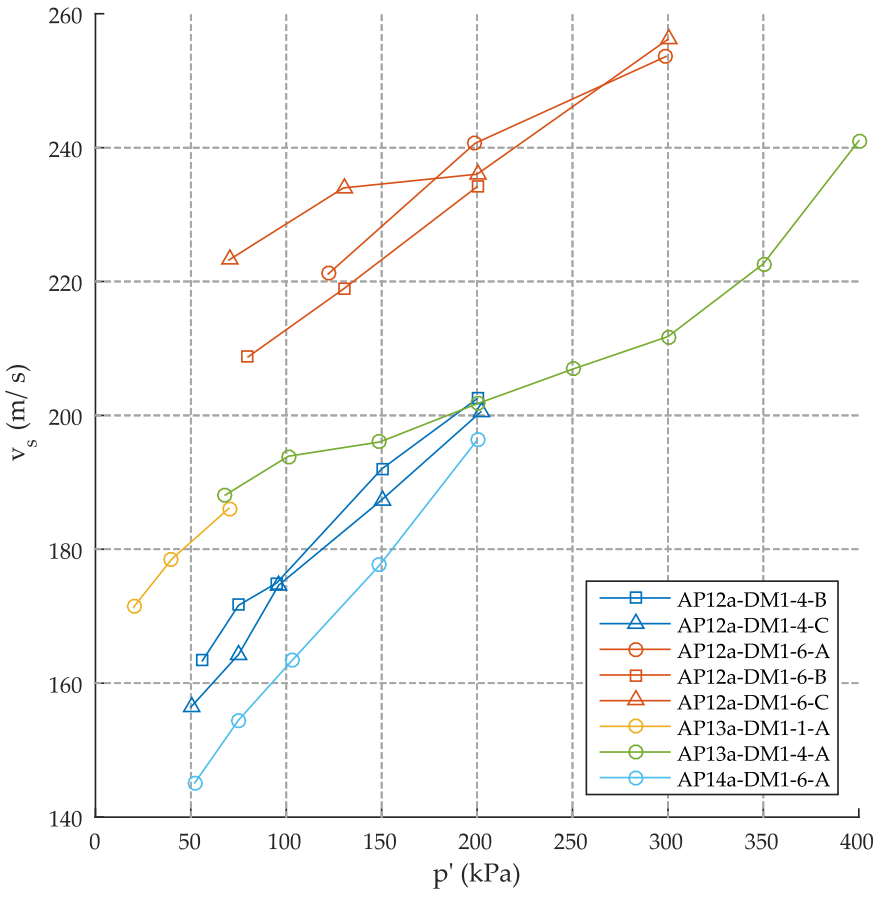


*Figure 7: Shear wave velocity measured during consolidation*

*Table 3: Summary of shear wave measurements*

| Sample | p' (kPa) | First Arrival (m/s) | | | Zero Crossing (m/s) | | | Difference (m/s) | | |
|---|---|---|---|---|---|---|---|---|---|---|
| | | 4kHz | 6kHz | 8kHz | 4kHz | 6kHz | 8kHz | 4kHz | 6kHz | 8kHz |
| AP12a-DM1-4-B | 56 | 164 | 163 | 163 | | 158 | 159 | | 5 | 4 |
| | 75 | 172 | 172 | 171 | | | | | | |
| | 95 | 177 | 176 | 173 | | | | | | |
| | 150 | 191 | 192 | 194 | | | | | | |
| | 200 | 202 | 203 | 203 | 203 | 204 | 203 | -1 | -1 | 0 |
| AP12a-DM1-4-C | 50 | 155 | 155 | 160 | 142 | 143 | 145 | 13 | 12 | 15 |
| | 75 | 165 | 166 | 162 | 152 | 156 | 158 | 13 | 10 | 4 |
| | 96 | 175 | 175 | 174 | 162 | 166 | 167 | 13 | 9 | 7 |
| | 150 | 187 | 187 | 188 | 162 | 166 | 167 | 25 | 21 | 21 |
| | 202 | 196 | 202 | 204 | 194 | 201 | 200 | 2 | 1 | 4 |
| AP12a-DM1-6-A | 122 | 217 | 224 | 222 | | 217 | 217 | | 7 | 5 |
| | 199 | 238 | 243 | 241 | | | | | | |
| | 299 | 253 | 253 | 254 | | 265 | 260 | | | |
| AP12a-DM1-6-B | 80 | 195 | 214 | 217 | 178 | 188 | 193 | 17 | 26 | 24 |
| | 130 | 214 | 221 | 221 | | | | | | |
| | 200 | 235 | 235 | 233 | 235 | 235 | 235 | 0 | 0 | -2 |
| AP12a-DM1-6-C | 70 | 210 | 227 | 233 | | | 206 | | | |
| | 130 | 230 | 235 | 237 | | | | | | |
| | 200 | 235 | 236 | 236 | | | | | | |
| | 300 | 255 | 256 | 257 | 254 | 265 | 260 | 1 | -9 | -3 |
| AP13a-DM1-1-A | 20 | 171 | 171 | 172 | | 173 | 169 | | -2 | 3 |
| | 40 | 179 | 179 | 178 | | | | | | |
| | 70 | 186 | 187 | 186 | | 190 | 186 | | -3 | 0 |
| | 40 | 179 | 179 | 178 | | | | | | |
| | 70 | 185 | 186 | 187 | | | | | | |
| AP13a-DM1-4-A | 68 | 189 | 188 | 188 | 185 | 188 | 187 | 4 | 0 | 1 |
| | 101 | 194 | 194 | 195 | | | | | | |
| | 149 | 197 | 195 | 195 | | | | | | |
| | 200 | 201 | 201 | 203 | 201 | 206 | 202 | 0 | -5 | 1 |
| | 250 | 207 | 207 | 207 | | | | | | |
| | 300 | 210 | 213 | 212 | | | | | | |
| | 350 | 223 | 223 | 222 | | | | | | |
| | 400 | 240 | 243 | 240 | 243 | 256 | 249 | -3 | -13 | -9 |
| AP14a-DM1-6-A | 52 | 145 | 145 | 145 | 135 | 142 | 143 | 10 | 3 | 2 |
| | 75 | 153 | 155 | 155 | | | | | | |
| | 103 | 163 | 164 | 163 | | | | | | |
| | 149 | 176 | 178 | 179 | | | | | | |
| | 200 | 196 | 195 | 198 | 195 | 200 | 197 | 1 | -5 | 1 |

## Cyclic Loading

For the purposes of this report, the criteria used to define "failure" is the number of cycles of a specific load amplitude required to cause a peak-peak axial strain (in any one cycle) of 5% or more.

The results are summarised in Figure 8 and Figure 9, with the same data being plotted on linear and log scales. The data has been split into the test series where the mean effective stresses were close to the in-situ vertical effective stress **(red markers)** and tests where the mean effective stress was close to 400kPa **(blue markers).** Additionally, different symbols have been used to distinguish between the different samples (i.e. different depths within the borehole).

In two cases, the sample did not reach the 5% axial strain failure condition, and have been plotted with markers which have been **shaded white**, and with the number of cycles set at 100. Markers which have been **shaded grey** indicate that the number of cycles to cause failure has been interpreted, and readers are directed to the appendix for the specific reasons.

For the tests conducted at a mean effective stress level of 400kPa, sufficient results are available to estimate a curve linking the cyclic resistance to the number of cycles of loading. This curve is shown as the dashed black line, and takes the form of Equation 5.

$$CRR = 0.3785N^{-0.096} \quad (5)$$

Specimens tested close to their estimated in-situ stress (AP13a-DM1-1 and AP13a-DM1-2 lie significantly above the points from tests conducted at 400kPa. It is striking that the points appear to fall on a much steeper line. While the number of tests is too low to draw definitive conclusions on the cyclic resistance of this material (failure reached in only 2 tests), a tentative relationship has been drawn with a red dashed line. This line is represented by Equation 6.

$$CRR = 1.45N^{-0.34} \quad (6)$$

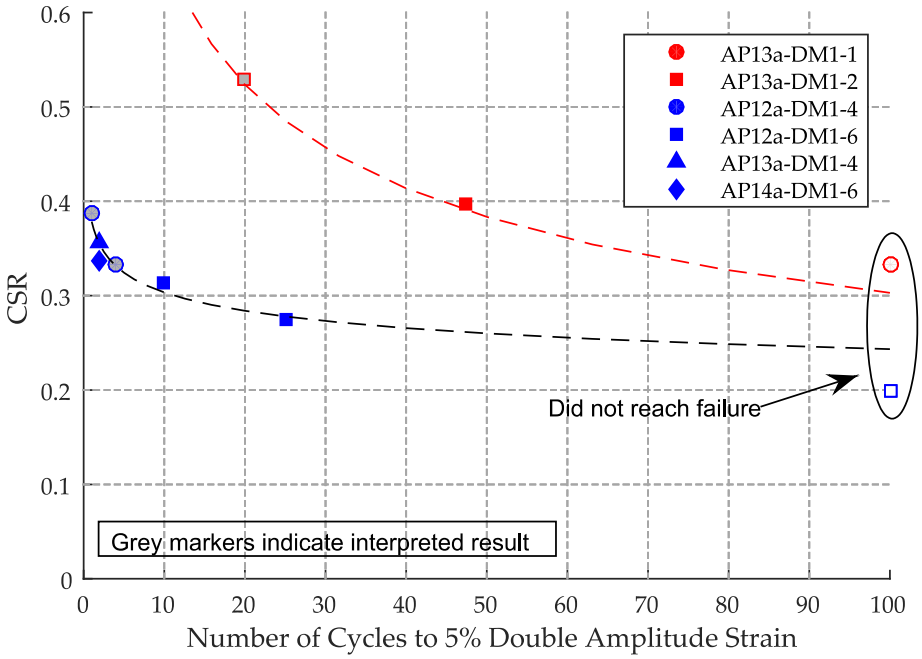


*Figure 8: Resistance to cyclic failure (linear scale)*

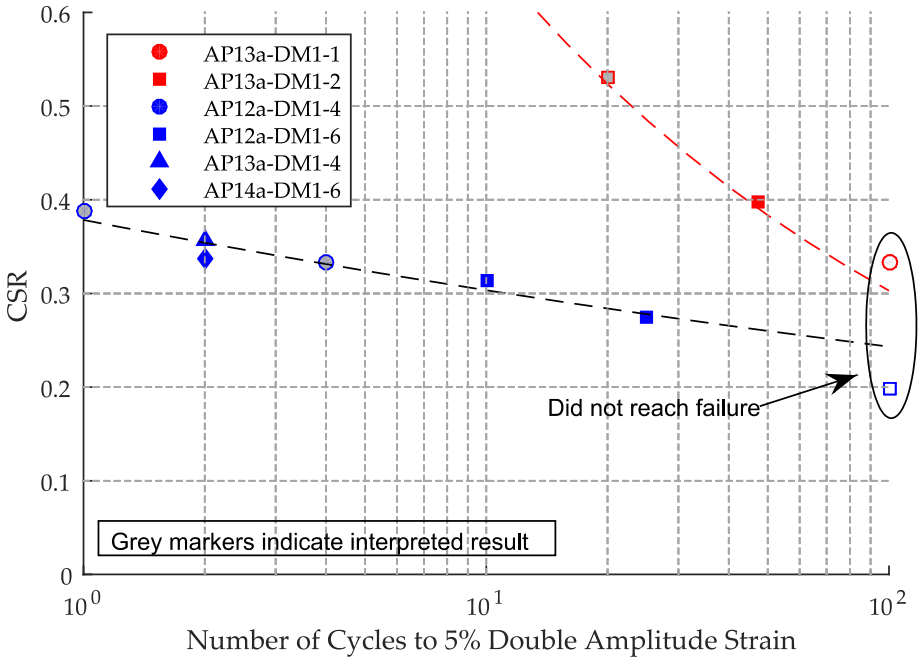


*Figure 9: Resistance to cyclic failure (log scale)*

A number of important aspects are apparent in both the summary figures 8 and 9, as well as the more detailed plots of test data shown in the testing appendices.

During cyclic loading, significant excess pore water pressures were generated. However, excess pore water pressure ratios ($r_u$) typically did not progress beyond 0.8 - 0.9 at the point of failure for the samples tested. There were two notable exceptions which occurred in the tests on material from AP13a-DM1-2 where $r_u$ exceeded 0.95. Aside from these two exceptions, the typical pore pressure response observed during the cyclic testing contrasts strongly with that of a sand undergoing liquefaction, where $r_u$ values in excess of 0.95 would typically be expected (Seed & Lee 1966). This pore pressure response is more similar to clay-like material undergoing cyclic softening, where $r_u$ values are often arrested at similar levels to those found in this testing programme.

Axial strains developed mainly on the extensional side of loading. This has been observed in a number of studies on undisturbed samples. However, an important feature of the strain development is that the specimens typically failed in a brittle manner once the level of axial strain reached 2-3%. Clear failure planes were observed during the testing (Figure 10 shows 2 examples), and in many cases caused extreme necking of the specimen (usually towards the middle of the specimen, as shown in Figure 10a). In the case of specimen AP12a-DM1-6C (Figure 10b), the failure caused a leak in the membrane, and the test was halted at that stage. When the specimen was removed from the apparatus, it was apparent that it had split into two distinct halves, with the failure plane at a relatively shallow angle to the horizontal (i.e. not on the plane of maximum shear stress). These behaviours suggest that in the cyclic tests, there were pre-existing defects (either cracks, or as a result of the assumed double porosity), which promoted brittle on the near-horizontal plane.

The relationship between CSR and number of cycles to failure appears to be reasonably well defined for the tests conducted at 400kPa and can be fitted to a power law model (Equation 5) in a similar way to the liquefaction resistance of sands ($CRR=aN^{-b}$). However, it should be noted that the “b” exponent

of 0.096 is relatively low. Sands typically have an exponent around 0.34, while the exponent for clays is typically much closer, in the region of 0.13-0.14 (Idriss & Boulanger 2008). Interestingly, the tests conducted at the estimated in-situ stress levels carry an exponent of 0.34, which is similar to that for sandy materials, though the multiplying factor, "a" is very high. It was previously noted that these tests also developed much larger excess pore water pressure.

Although it might be possible to describe these specimens as undergoing a cyclic failure, it is clearly different to liquefaction. **The brittle nature of the specimen failures is an issue of engineering importance**, since it implies that if the material is loaded (seismically or otherwise), then a sudden failure mechanism could develop, with large displacement occurring very quickly, and without time for remediation. **Whether this failure mechanism could develop would depend significantly on the overall soil profile, and in particular, how extensive the soils being tested are across the site. The potentially brittle failure as well as the extent of these soils should be considered in the overall assessment of stability.**

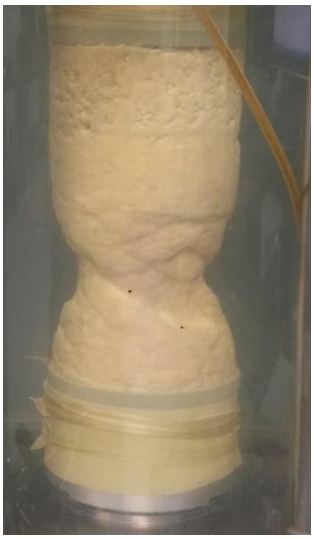

(a) Necking of specimen AP12a-DM1-4-A

(b) Failure plane on specimen AP12a-DM1-6-C

*Figure 10: Post-failure appearance of specimens*

## Post Cyclic Testing

After cyclic testing was completed, samples were either subjected to an undrained triaxial test, or were reconsolidated back to their original mean effective stress level. These results are summarised in Table 4 and Table 5. Noted that specimens AP12a-DM1-6 B and C both developed tears in the membrane when the sample failed during the cyclic loading. No post-cyclic test data is therefore available for these specimens.

It should be noted that the deviator stresses shown in Table 4 assume that the specimen deforms as a right cylinder. Reference to the deformed shape of the tested specimens (see photos in the appendix) indicates that this is clearly not the case for all specimens, and some error is therefore associated with these stress values due to the necking at the end of cyclic loading (these specimens are denoted with an asterisk in Table 4). Axial strains are given relative to the start of the post-cyclic testing phase. The angle of friction shown in Table 4 is estimated according to Equation 7.

$$sin\phi = \frac{3q}{6p'+q} \tag{7}$$

The volumetric strains during reconsolidation are shown for 2 specimens in Table 5, along with the maximum axial strain and shear strain during the cyclic loading phase of the test. The maximum shear strain has been calculated for undrained test conditions according to Equation 8.

$$\gamma_{cyclic,max} = 1.5\varepsilon_{a\ cyclic,max} \tag{8}$$

*Table 4: Post-cyclic CIU test summary*

| | | Peak | | | | Ultimate | | | |
|---|---|---|---|---|---|---|---|---|---|
| Specimen | Load rate (mm/min) | $\varepsilon_a$ (%) | $p'$ (kPa) | $q$ (kPa) | $\phi$ (°) | $\varepsilon_a$ (%) | $p'$ (kPa) | $q$ (kPa) | $\phi$ (°) |
| AP12A-DM1-4-A* | 1 | 18.8 | 120.8 | 192.5 | 39 | 18.8 | 120.8 | 192.5 | 39 |
| AP12A-DM1-4-C† | 0.03 | 6.0 | 134.9 | 220.3 | 39.9 | 23.3 | 120.4 | 185.7 | 37.8 |
| AP12A-DM1-6-A† | 1 | 0.9 | 227.3 | 344 | 37.2 | 23.2 | 144.2 | 227 | 38.6 |
| AP13A-DM1-2-B†‡ | 1 | 5.2 | 42.6 | 96.4 | 55.2 | 17.0 | 35 | 72.2 | 50.1 |
| AP13A-DM1-4-A* | 1 | 23.4 | 121.7 | 193.6 | 39 | 23.4 | 121.7 | 193.6 | 39 |
| AP14A-DM1-6-A* | 0.03 | 27.0 | 93.6 | 150.6 | 39.4 | 27.0 | 93.6 | 150.6 | 39.4 |

*: specimen necked during cyclic loading.
†: double amplitude axial strains did not reach 5% during cyclic loading
‡: test pressure is lower than yield stress

*Table 5: Volumetric Strains during reconsolidation*

| Specimen | $\varepsilon_{a\ cyclic,max}$ (%) | $\gamma_{cyclic,max}$ (%) | $\varepsilon_{vol,reconsol}$ (%) |
|---|---|---|---|
| AP13a-DM1-1-A | 0.15 | 0.23 | 0.08 |
| AP13a-DM1-2-A | 7.1 | 10.6 | 1.6 |

## CIU Testing

One undrained monotonic test was carried out to understand the response of the material from the AP14a-DM1-6 relative to the samples collected in other tubes.

The results have been processed in a similar way to the post-cyclic CIU tests previously described, with the summary parameters shown in Table 6 below.

*Table 6: CIU testing summary.*

| | | Peak | | | | Ultimate | | | |
|---|---|---|---|---|---|---|---|---|---|
| Specimen | Load rate (mm/min) | $\varepsilon_a$ (%) | $p'$ (kPa) | $q$ (kPa) | $\phi$ (°) | $\varepsilon_a$ (%) | $p'$ (kPa) | $q$ (kPa) | $\phi$ (°) |
| AP14A-DM1-6-B | 0.03 | 12.6 | 208.5 | 214.4 | 26.0 | 22.5 | 117.9 | 160 | 33.6 |

# References

Idriss, I.M. & Boulanger, R.W. (2008) *Soil liquefaction during earthquakes*. Monograph MNO-12, Earthquake Engineering Research Institute. Oakland, CA.

Seed, H.B. & Lee, K.L. (1966) Liquefaction of saturated sands during cyclic loading. *J. Soil mechanics and foundations division.* **92**(SM6):105-134

Singh, S., Seed, H.B. & Chan, C.K. (1982) Undisturbed sampling of saturated sands by freezing. *Journal of the geotechnical engineering division.* 108(GT2): 247-264.

Skempton, A.W. (1954) The pore-pressure coefficients A and B. *Geotechnique.* **4**(4):143-147